Ice discharge of eastern Dome C drainage area, Antarctica, determined from airborne radar survey and satellite image analysis

Massimo Frezzotti,[1] Ignazio Ezio Tabacco,[2] Achille Zirizzotti[3]
[1]*ENEA, Via Anguillarese 301, I-00060 S. Maria di Galeria–Rome, Italy*
[2]*Dipartimento di Scienze della Terra, Università degli Studi di Milano, Via Cicognara 7, I-20124 Milan, Italy*
[3]*Istituto Nazionale di Geofisica, Via di Vigna Murata 605, I-00143 Rome, Italy*

ABSTRACT. Eastern Dome C, southern Talos Dome and northern Taylor Dome are drained by the Priestley, Reeves, David, Mawson and Mackay outlet glaciers, which flow into the Scott Coast on the west side of the Ross Sea, Antarctica. Airborne radar surveys were conducted on these glaciers to determine ice thickness and bed morphology along transverse and longitudinal profiles of the grounded and floating segments. A new analysis of a Landsat Thematic Mapper satellite image using a tracking technique was used to measure ice velocity at grounding lines and along ice tongues. The integration of radar and satellite data helped to locate grounding lines and to calculate the ice discharge. Changes in ice fluxes of floating glaciers were used to determine basal melting and freezing rates. The ice discharge calculated is less than half that required for a zero net surface mass balance according to the inputs given by the accumulation estimates widely adopted at present. The basal melting rates of meteoric ice represent 50% of the net ablation rate.

INTRODUCTION

The mass balance of the Antarctic ice sheet is determined by the difference between net snow accumulation and ice discharge across the grounding line into the ocean. About 90% of the snow that falls inland is drained by outlet glaciers and ice streams (Morgan and others, 1982). Velocity and thickness of glaciers at the grounding line determine the rate at which the drainage area releases mass to the ocean. Despite the availability of data on snow accumulation, ice velocities, surface and basal melting and iceberg discharge, it is difficult to determine the present-day mass balance of the ice sheet (Bentley and Giovinetto, 1991; Jacobs and others, 1992; Vaughan and others, 1999). Eastern Dome C, southern Talos Dome and northern Taylor Dome are drained by the Priestley, Reeves, David, Mawson and Mackay outlet glaciers, which flow into the Scott Coast on the west side of the Ross Sea (Fig. 1). The ice discharge and drainage area of these outlet glaciers has until now been unknown. Remote-sensing techniques have been used to study the iceberg calving flux of the Scott Coast during the 20th century (Frezzotti and Mabin, 1994; Frezzotti, 1997), but this earlier work did not determine the basal melting/freezing rates of floating glaciers (ice tongues, glacier tongues, ice shelves) which fringe the Victoria Land coast. Although the melting pattern under a floating glacier is complex, the basal melting rate can be derived from surface measurements if the floating glacier is assumed to be in a steady state, as we show here.

A new digital elevation model (DEM) of the eastern Dome C area, derived from satellite radar altimetry (Rémy and others, 1999), is used to define the drainage basins more accurately.

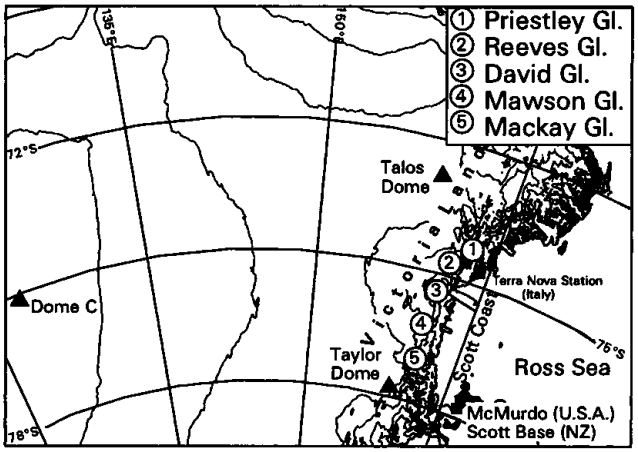

Fig. 1. Location of eastern Dome C drainage area and Priestley, Reeves, David, Mawson and Mackay Glaciers.

During the 1995/96 and 1997/98 Italian Antarctic Expeditions, an airborne radar survey was conducted on the grounded and floating portions of outlet glaciers. The radar survey provided data on ice thickness and bed morphology along transverse and longitudinal profiles of the outlet glaciers and their floating portions.

In this paper, surface-feature tracking techniques on sequential satellite imagery (Bindschadler and Scambos, 1991; Frezzotti and others, 1998a) are used to analyze 1990 and 1992 Landsat Thematic Mapper (TM) imagery, providing measurements of ice velocity at the grounding line and along floating areas. By integration of radar and satellite data the grounding line of outlet glaciers is identified and ice discharge is estimated. The calculated ice discharge was compared to the net surface balance determined by Giovinetto and Bentley

(1985), McIntyre (in Swithinbank, 1988) and Vaughan and others (1999). Changes in ice fluxes of floating glaciers were used to determine basal melting and freezing rates.

METHODOLOGY

Ice-thickness measurements

Radar surveys were conducted during the 1995 and 1997 Antarctic seasons (Fig. 2). The radar equipment used in 1995 (Tabacco and others, 1998) includes a digital pulse generator that creates a 60 MHz pulse of controlled duration (0.3 or 1.0 μs), at about 1 mW peak power. A solid-state power amplifier raises that to >2 kW peak power. The receiver consists of a solid-state low-noise pre-amplifier and a controlled bandwidth successive detection logarithmic amplifier. The dynamic range of the amplifier is 80 dB, and the output is digitized (by means of a 10 MHz digital oscilloscope) to eight-bit resolution, acquiring 512 samples every 100 ns ($\pm$8 m accuracy in ice-depth determination) for a total of 51.2 μs. The system allows an acquisition rate of one record every 3 s. The calibration test of the overall system shows a system performance of 150–160 dB (not including antenna gain), depending upon pulse length and bandwidth settings. The radar equipment was deployed by a Twin Otter aircraft, with folded dipole radar antennas under each wing, one for transmittal, the other for reception. Antenna gain is estimated to be 8.2 dB. A global positioning system (GPS) Trimble 4000SSE system (L1 and L2 frequency), with a geodetic antenna mounted on the fuselage, was installed and linked to the radar. A master GPS station, synchronized with the rover, was installed at Terra Nova station to enable differential correction of data. In 1997, improvements were made to the system's hardware and software. Relevant changes were made to the acquisition unit, the radio-frequency and control unit and the software. A new digitizing board, based on an eight-bit 20 MHz analog/digital flash converter and Fast integrated-circuit components, was developed, along with related software. The sampling rate of the analog signal was doubled to 1024 samples every 50 ns, so as to increase the accuracy of ice-depth determination ($\pm$4 m). The new system, with a 166 MHz Pentium-based personal computer and a TX trigger pulse repetition rate of 50 Hz, allows an acquisition rate of ten records every second.

The survey was completed in four flights (two in 1995 and two in 1997), with a cruise speed of 100–120 kt (185–220 km h^{-1}) and an average altitude of 1000 ft (300 m; controlled by radar altimeter). In 1995 the data-acquisition rate was every 150–185 m; in 1997 the acquisition rate was every 5–6 m. A synchronized GPS with $\pm$20 m precision in x, y coordinates (only pseudo-range differential corrections were made) was used to geo-reference the radar data. Priestley, Reeves, David and Mawson Glaciers were surveyed to determine the grounding line of each (by means of longitudinal profiles) and to evaluate ice thickness along floating portions of the ice tongues (by means of transverse profiles). A total of 35 radar profiles were made: 3 longitudinal and 4 transverse at Priestley Glacier, 3 longitudinal and 2 transverse at Reeves Glacier, 4 longitudinal and 11 transverse at David Glacier–Drygalski Ice Tongue, and 2 longitudinal and 6 transverse at Mawson Glacier. All radar profiles were processed with a software package specially designed for the new radio-echo sounder. A constant electromagnetic wave propagation velocity of 168 m μs^{-1} was assumed. Thickness was determined to the nearest digital sample on the record with a digitizing error of $\pm$100 ns (1995) and $\pm$50 ns (1997) for both surface and bed reflections. This corresponds to a rms uncertainty in thickness of about $\pm$16 m (1995) or $\pm$8 m (1997). Ice-thickness data at each intersection of longitudinal and transverse profiles were compared; measurements differed by $<$10 m, i.e. less than the estimated accuracy in thickness determination. By combining 1995 and 1997 data, it was possible to determine the ice thickness and to locate the grounding line of the surveyed glaciers.

Surface velocity measurements

Several investigators have shown that ice-flow velocities can be determined by measuring the displacement of features observed in pairs of visible or synthetic-aperture radar images (e.g. Morgan, 1973; Lucchitta and Ferguson, 1986; Bindschadler and Scambos, 1991; Lucchitta and others, 1993, 1995; Bindschadler and others, 1996; Frezzotti and others, 1998a). Landsat TM 4 and 5 (1990–92) images of Priestley, Reeves, David and Mawson Glaciers, Drygalski Ice Tongue and the Nansen Ice Sheet, and SPOT 1 XS (1988) images of Reeves and Priestley Glaciers and the Nansen Ice Sheet were acquired. All images were provided in digital format on computer tape and were processed to eliminate scan-lines in each spectral band. A first-principal-component image was generated to enhance the surface features of glaciers and to reduce image noise (Bindschadler and Scambos, 1991). New displacement velocities were measured by comparing the 1990 Landsat TM reference image with the 1988 SPOT XS and the 1992 Landsat TM images. Images were co-registered using 19 tie points for the 1990 and 1992 Landsat TM data of David–Drygalski, Priestley and Mawson Glaciers, and 20 points for the 1992 Landsat TM and 1988 SPOT XS imagery of Reeves Glacier. Small rock outcrops (a few pixels in size) near the glaciers, at low elevation and widely scattered across the velocity-measurement area, were chosen as image tie points. Images were co-registered using a first-order polynomial, and the data were resampled using a cubic convolution algorithm to a common pixel size of 28.5 m (that of the reference image). Residual errors from the co-registration process range from the two-pixels to sub-pixel level. Because Drygalski Ice Tongue extends some 90 km out to sea, co-registration errors may increase to the east along the ice tongue where there are no fixed features to be used as tie points. The displacement of surface features (crevasses, ice fronts, snowdrifts, drift plumes, etc.) in sequential images was determined using a semi-automatic procedure. Distinct features that occur in both images were identified first, then a 16 pixel by 16 pixel image chip containing a feature was extracted from each image. A comparator then determined the relative location of the feature in the two chips to a 1/4 pixel accuracy. Based on the measured feature displacement, the known time gap between images and image pixel size (28.5 m), the average velocity of each feature point was calculated in image coordinates. The time gaps for the different image pairs vary from 2 to 4 years. A total of 750 points were measured on the 1990 and 1992 Landsat TM images of David Glacier–Drygalski Ice Tongue; 650 points in the 1988 SPOT XS and 1992 Landsat TM images of Reeves Glacier–Nansen Ice Sheet; and 430 and 100 points in the 1990 and 1992 Landsat TM images of Priestley and Mawson Glaciers, respectively.

Satellite image maps, with 30 m pixel spatial resolution, were created using the Landsat TM reference image (Fig. 2).

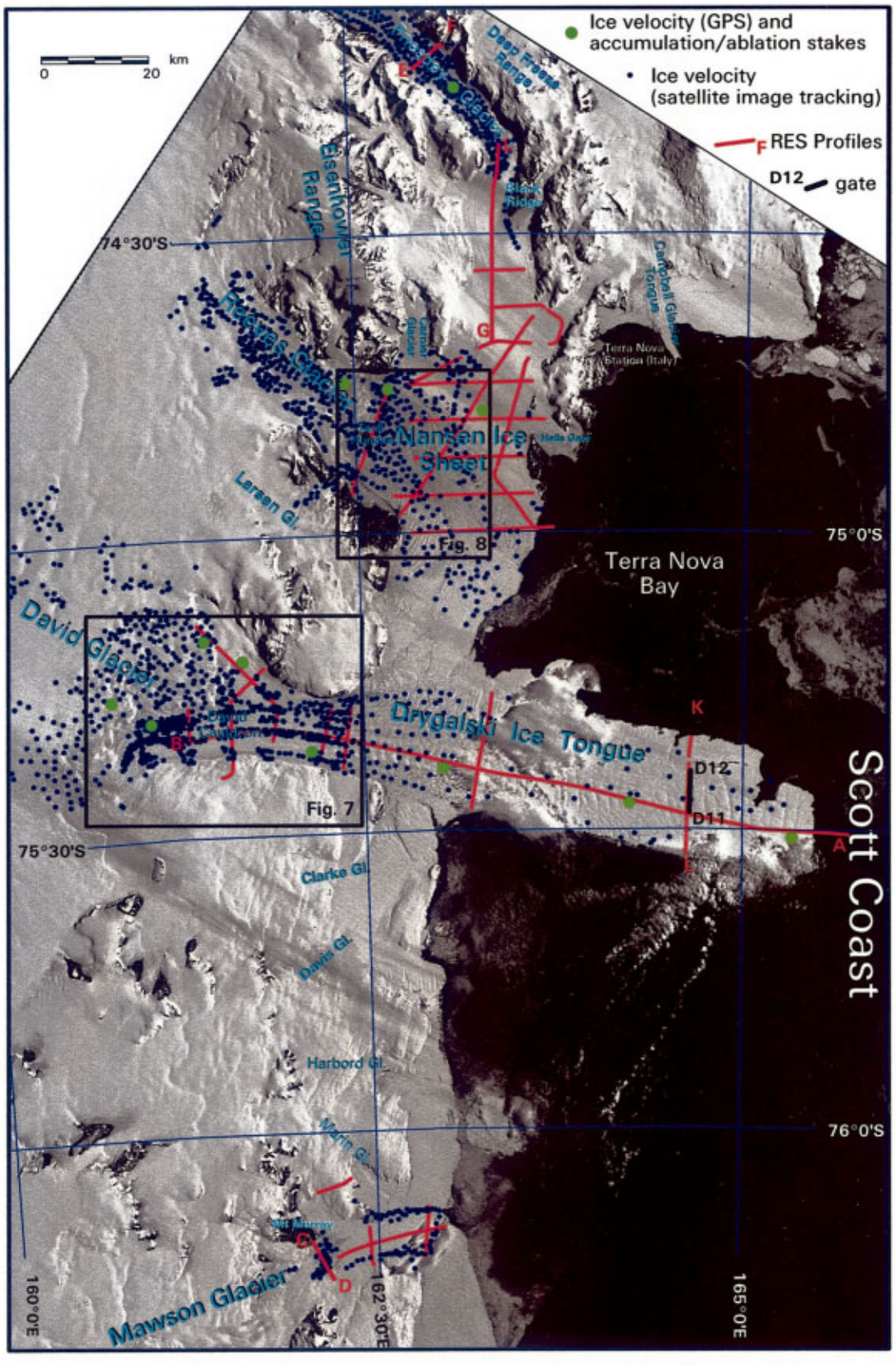

Fig. 2. Landsat TM satellite image map with positions and name of RES profiles, velocity data points determined by tracking technique and GPS, location of accumulation/ablation stakes, position and name of gate and location of Figures 7 and 8.

The image was geo-referenced by identifying image points corresponding to 15 ground-control points established by the Italian Antarctic Research programme with GPS surveys. The image was rectified to a Lambert Conformal Conic cartographic projection by using a linear conversion matrix, with a rms error of about two pixels. The same conversion matrix was applied to the satellite-image velocity points, which were rectified to the same projection. Frezzotti and others (1998a) have shown that flow rates derived from the analysis of satellite imagery compare well with those obtained from GPS measurements of Priestley, Reeves and David Glaciers. When compared to GPS measurements in areas close to image tie points, the error in average velocity measurements using feature tracking may be as little as

± 15–$20\ \mathrm{m\ a^{-1}}$ (e.g. grounding-line area). In areas far from tie points, such as the outer part of Drygalski Ice Tongue, the two types of measurements differ by about $\pm 70\ \mathrm{m\ a^{-1}}$.

Ice flux

The co-registration of airborne radar data and satellite imagery was based on geographic coordinates. In regions with gaps in velocity (e.g. ice margins) or ice-thickness data (e.g. close to valley walls), dummy values were kept consistent with other data (velocity or ice thickness) and with our reconstruction of the morphology of the glacier bed and margin. To calculate the ice-equivalent volume flux (F) at the grounding line and along flow transects, Equation (2) (modified) of Bindschadler and others (1996) was used:

$$F = \sum_{w} V_{\mathrm{t}} H \Delta w, \qquad (1)$$

where w is the width, V_{t} is the velocity component perpendicular to the transect, H is the ice thickness and Δw is the increment in width (Table 1).

Since we do not know how the ice velocity varies with depth inland, ice flux was measured only close to the grounding line and along the floating part of the glacier, where it can safely be assumed that the velocity is constant with depth. Where radar surveys were not perpendicular to the flow across a gate, a projection of the nearest ice-thickness measurement was used. The grounding lines of outlet glaciers were surveyed using satellite imagery and radar data by identifying linear transverse depressions and change in surface slope that cut across glaciers in the satellite images

Table 1. Ice discharge of outlet glaciers and data for each glacier, including width (W), average value of velocity ($\bar{V}_{\mathrm{t}}$), average ice thickness ($\bar{H}$) and ice discharge computed from Equation (1)

Outlet glacier		W	$\bar{V}_{\mathrm{t}}$	$\bar{H}$	*Ice discharge*
		km	$\mathrm{m\ a^{-1}}$	m	$\mathrm{km^3\ a^{-1}}$
Priestley		8.2	93	1008	0.77 ± 0.13
Reeves		16.9	109	659	0.52 ± 0.06
	northern flow	9.8	113	774	0.9 ± 0.1
David					
	southern flow	10.0	461	1000	6.9 ± 0.6 [1]
Mawson		7.9	138	463	0.52 ± 0.07
Mackay		4.1	265	300	0.33 ± 0.06 [2]
Total					10.0 ± 1.0

[1] Calculated value from ice discharge at EF section ($5.0 \pm 0.2\ \mathrm{km^3\ a^{-1}}$) plus continental ice melted ($1.9 \pm 0.4\ \mathrm{km^3\ a^{-1}}$) between grounding line and section EF (Fig. 7).

[2] From Frezzotti (1997).

and bottom crevasses in the radar profiles. Figure 3a shows the Drygalski Ice Tongue longitudinal profile AB surveyed by radar, with features characteristic of bottom crevasses observed about 130 km from the ice front. Ice thickness ranges from 200 to >1500 m.

Annual surface-accumulation/ablation rates along Drygalski Ice Tongue and the Nansen Ice Sheet were collected between 1991 and 1995 using a stake network (Fig. 2). Those data show spatial variation due to aeolian processes induced by katabatic winds descending from the plateau to Terra

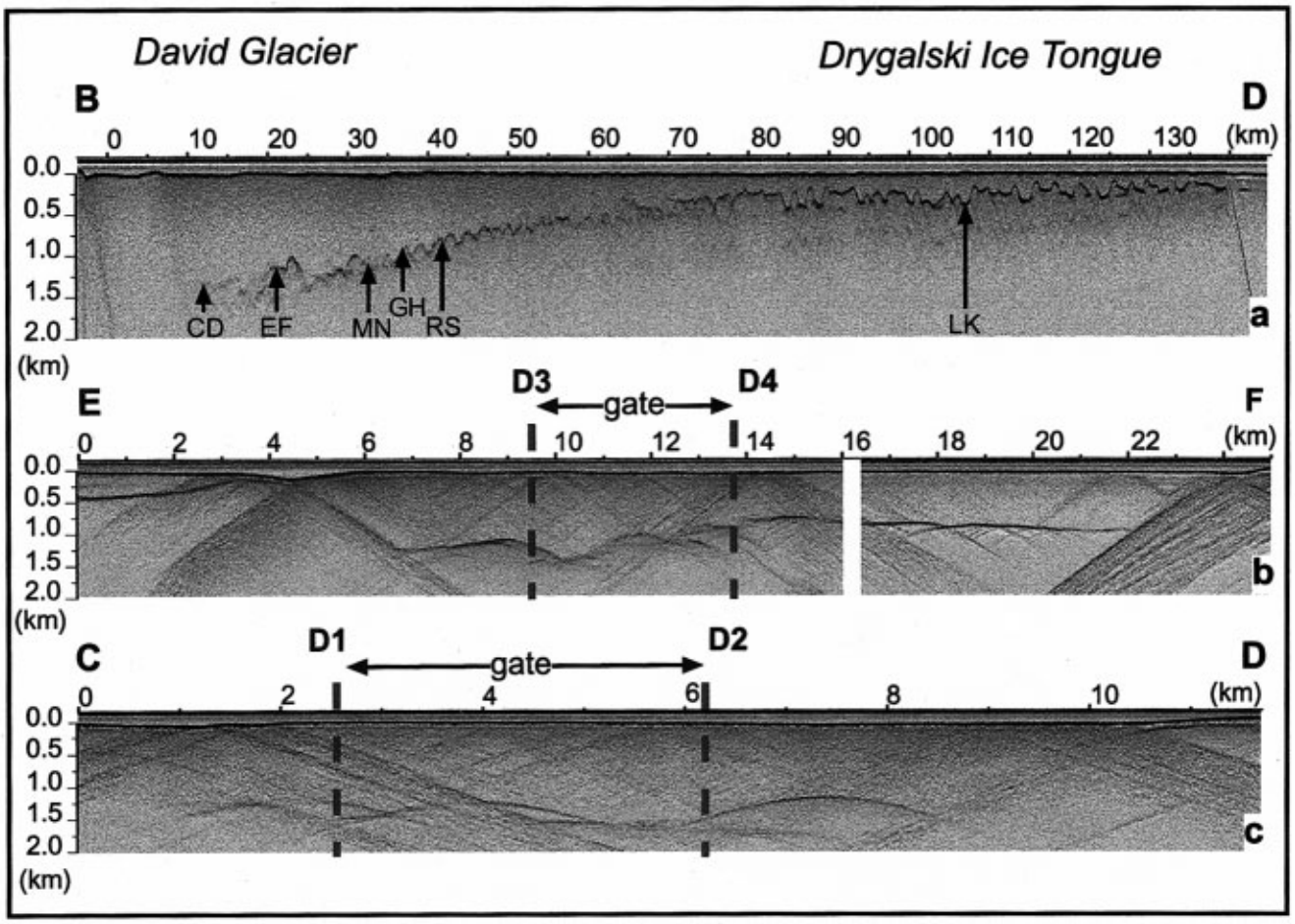

Fig. 3. Radar profiles of David Glacier and Drygalski Ice Tongue. (a) Longitudinal profile BD; arrows indicate the position of transversal. (b, c) Transversal radar profiles EF and CD; vertical lines indicates the position of the "gate-limited" width. Profile positions in Figures 2 and 7.

Nova Bay (Frezzotti, 1993, 1998). Accumulation/ablation data from the stake network were extrapolated over flux gates using Landsat TM image observations of accumulation/ablation-rate indicators (blue ice, surface morphology, etc.).

The flow margins of the Nansen Ice Sheet and David Glacier–Drygalski Ice Tongue were surveyed through satellite image analysis. Discharge fluxes across flow bands (termed "gates" in this paper) along the Nansen Ice Sheet and Drygalski Ice Tongue were calculated to determine basal melting and freezing rates; rates for regions bounded by two gates and a flow margin were calculated by summing the upstream gate flux with the surface accumulation/sublimation flux, and subtracting the downstream gate flux using equation (3) (modified) of Bindschadler and others (1996):

$$m - \delta H/\delta t = (F - F' + A)/S, \qquad (2)$$

where m is melt rate, $\delta H/\delta t$ is the rate of thickness change, F and F' are the up- and downstream fluxes, A is the surface flux and S is the flow-band surface area.

Drainage area

Drainage was mapped using a DEM of Antarctica provided by Rémy and others (1999). The DEM was derived from the two geodetic 168 day repeat orbits of the European remote-sensing satellite (ERS-1) radar altimeter. Rémy and others (1999) have analyzed the waveform altimetry data from geodetic orbits to create maps with a 1/30° grid size. The DEM has better than 1 m accuracy over the parts of East Antarctica where slope gradients are <0.5%. Around Victoria Land, where slopes are steeper, tracking was not continuous due to loss of tracking, so altimetry data were integrated with data from digitized U.S. Geological Survey (USGS) reconnaissance maps of Antarctica at a 1:250 000 scale. By integration of the DEM with digitized USGS data, a new DEM of the study area, with a Lambert Equal Area projection and a grid size of 1 km, was created. The catchment basin was delineated by applying standard hydrological modelling tools included in the proprietary GIS ARC/info (version 7.2) to the new DEM; results are similar to those of Vaughan and others (1999). The grounded basin area was calculated taking into account the new grounding line inferred from the analysis of satellite imagery and radio-echo sounding (RES) data.

DISCUSSION

Drainage area

Priestley and Reeves Glaciers (Figs 2 and 4) drain the south-eastern portion of the Talos Dome area and part of the northern Victoria Land névé (southern part of the Deep Freeze and Eisenhower Ranges). David Glacier, the largest outlet glacier in Victoria Land, drains the inner part of the plateau flowing from eastern Dome C, southern Talos Dome and northern Taylor Dome. Mawson and Mackay Glaciers flow through the Scott Coast and drain the northern peripheral portions of Taylor Dome and local ice originating within a few tens of kilometres of the Transantarctic Mountains.

On the DEM constructed, the estimated size of the drainage basin of these outlet glaciers is 235 000 km^2. Figure 4 shows a direct comparison between drainage basins derived by Giovinetto and Bentley (1985) and those derived as above. Our drainage results are similar to those of Vaughan and others (1999). The drainage basin derived from the DEM is different close to Dome C from that derived by Giovinetto and Bentley (1985) on the basis of historical data (Drewry, 1983); the catchment area ends 300 km short of the Dome C culmination. The first 300 km of the eastern Dome C drainage area flows into the Ross Ice Shelf and not into the Scott Coast, as suggested by Drewry (1983) and Giovinetto and Bentley (1985). Drainage system e-d-d′-D″-E (Fig. 4) of Giovinetto and Bentley (1985) and Vaughan and others (1999) includes the McMurdo Dry Valleys region, the largest ice-free area in Antarctica, which is not considered in this paper. Along the Scott Coast there are other glaciers (Marin,

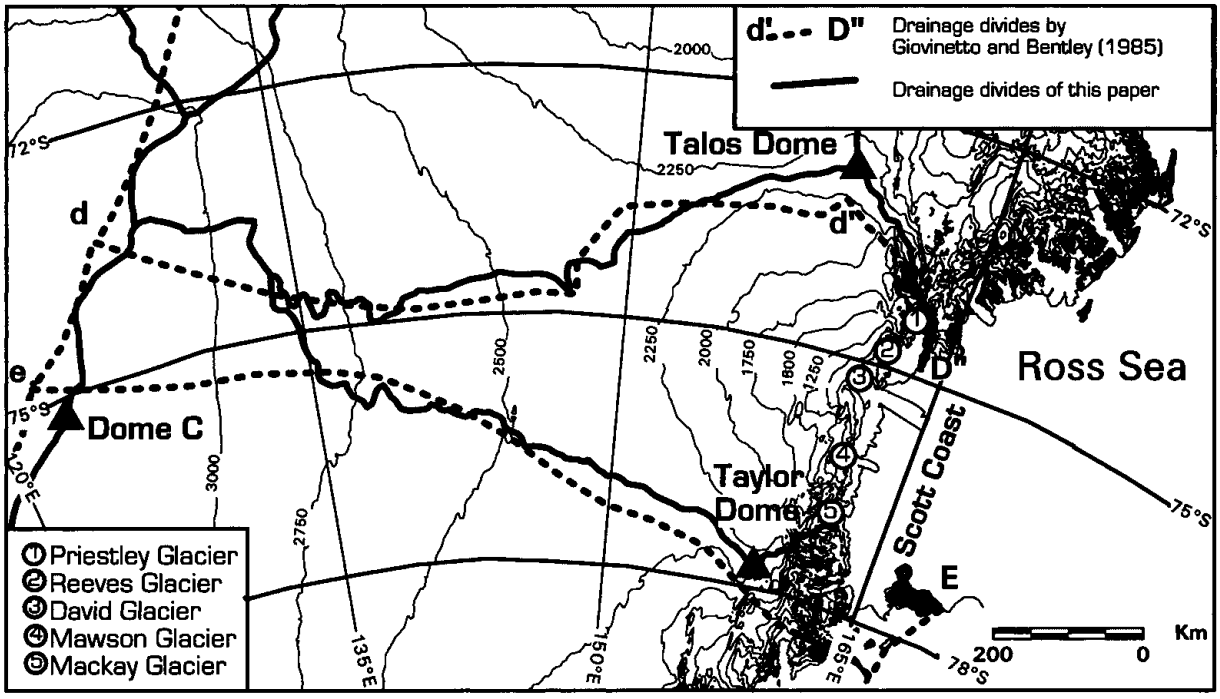

Fig. 4. Delineation of drainage area of Priestley, Reeves, David, Mawson and Mackay Glaciers. Dotted lines indicate drainage system (e-d-d′-D″-E) drawn by Giovinetto and Bentley (1985).

Harbord, Davis, Clarke and Larsen; Fig. 2) which drain a small area of local nunataks of about 5250 km^2. The ice thickness of these glaciers is not available at the grounding line and they are not considered in this paper.

Outlet-glaciers discharge

Priestley and Reeves outlet glaciers occupy deep troughs (Fig. 2) that stem from cirques cut into the bedrock beneath inland ice (Orombelli and others, 1991). Reeves and Priestley Glaciers merge and form the Nansen Ice Sheet (the name given by the first explorers, although it is technically an ice shelf). The grounding lines of these glaciers were mapped by Frezzotti and others (1996) using satellite imagery; the grounding-line locations have been confirmed by the new radar data. Frezzotti and others (1996) place the grounding line of Priestley Glacier close to Black Ridge, about 62 km from the ice front of the Nansen Ice Sheet. An ice-thickness transect of Priestley Glacier was made 15 km upstream of the grounding line. At this transect (Fig. 5a) the ice is >1000 m thick and ice velocity reaches 130 m a^{-1}. The ice velocity was calculated using new satellite-image tracking and was confirmed by GPS measurements (Frezzotti and others, 1998a). Based on these data, the estimated ice discharge of Priestley Glacier is 0.77 ± 0.13 km^3 a^{-1} (Fig. 6; Table 1).

Where Reeves Glacier flows into the Nansen Ice Sheet it separates into two streams because of interaction with Teall Nunatak (shown later, Fig. 8) and with buried topography (Baroni and others, 1991). Frezzotti and others (1996) located the grounding line just at Teall Nunatak, about 40 km upstream of the front of the Nansen Ice Sheet. Figure 5b illustrates the radar cross-section of Reeves Glacier close to the grounding line, acquired during the 1995 expedition. In spite of the low horizontal resolution (1 record/170 m), ice thickness can be measured along the whole section. The feature at 10 km is Teall Nunatak which splits the ice-flow discharge. At the grounding line the ice is up to 700 m thick and ice velocity reaches 200 m a^{-1} (Fig. 6; Table 1). Ice-thickness and velocity data (satellite tracking confirmed by GPS) are known across the grounding line, and ice discharge is calculated to be 0.52 ± 0.06 km^3 a^{-1}.

David Glacier is the main outlet glacier of Victoria Land, coinciding with a subglacial trench which crosses the Transantarctic Mountains, and linking the Ross Sea basin with the internal Wilkes subglacial basin (Steed and Drewry, 1982). As most of David Glacier basin is below sea level, it is considered to be a marine-based glacier (Orombelli, 1991). David Glacier is fed by two main flows, a northern one from Talos Dome and the major southern flow from Dome C (Frezzotti, 1993). Satellite images and GPS measurements show that the southern flow is formed by the convergence of three ice streams under an icefall, the David Cauldron (Fig. 7). Satellite images display three ice streams separated by heavily crevassed shear zones from ridges of slow-moving ice on either side. These ice streams have widths of >10 km within 150 km of David Cauldron. Based on GPS measurements, ice velocities within these flows are 50–100 m a^{-1}, whereas ice velocities outside the flows are 20–27 m a^{-1} (personal communication from L. Vittuari, 1998). At David Cauldron the streams enter a deep fjord-like valley (McIntyre, 1985). Frezzotti (1993) found that the grounding line is about 50 km inland from the coast, where transverse depressions, characteristic of a rapidly spreading flow in the floating glacier, can be seen in satellite

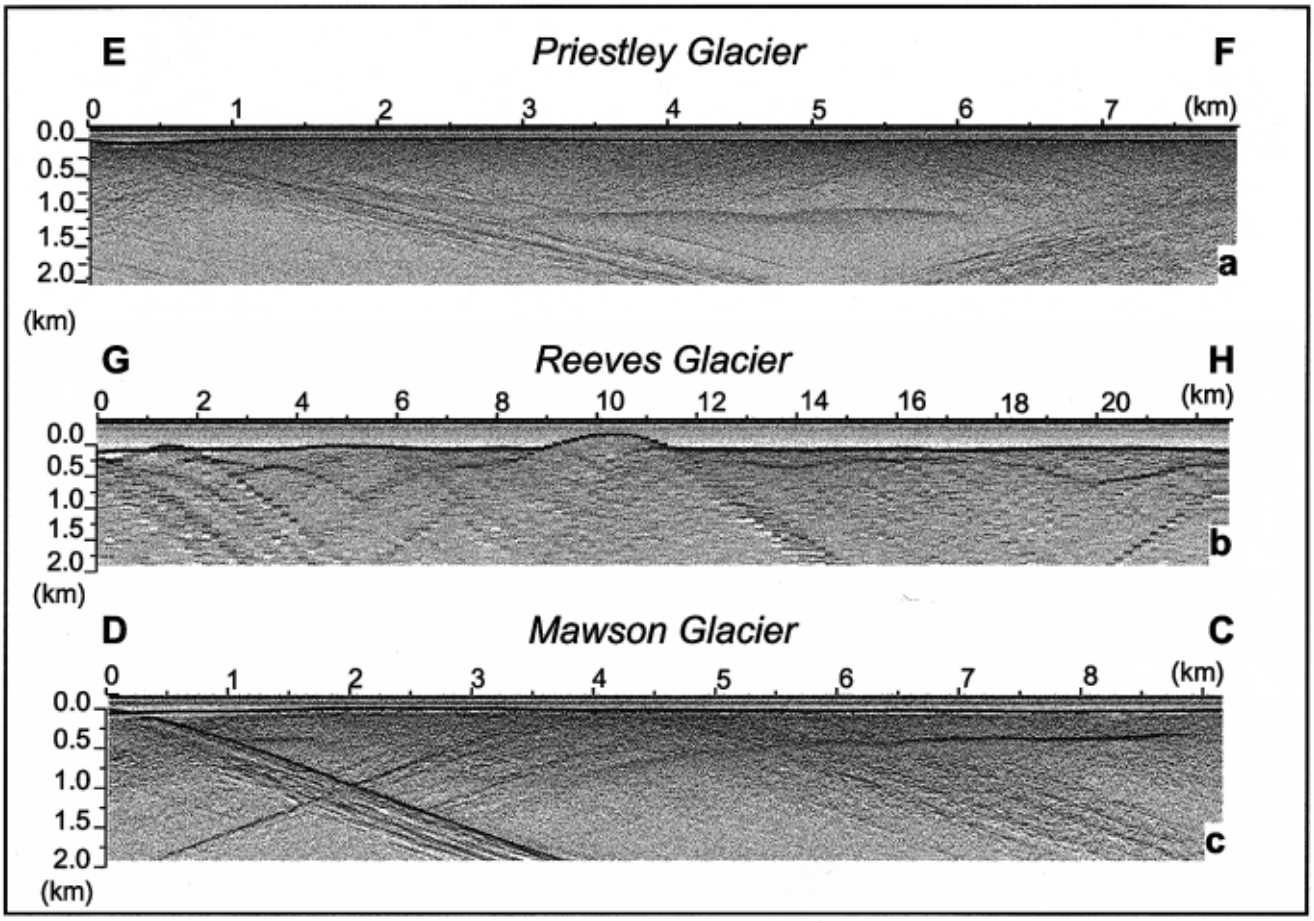

Fig. 5. Radar profiles of Priestley (a), Reeves (b) and Mawson (c) transects; profile positions in Figures 2 and 8.

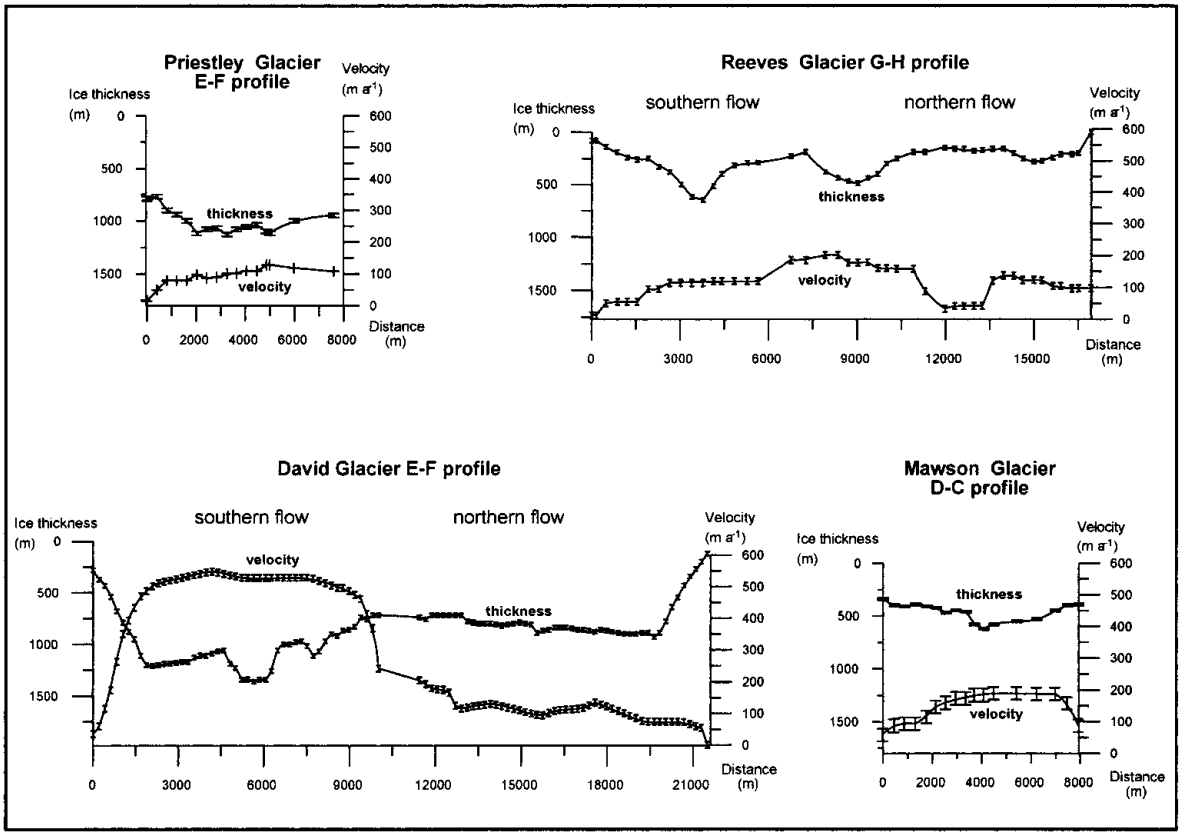

Fig. 6. Four transects of ice thickness and surface velocity of Priestley, Reeves, David and Mawson Glaciers.

imagery (Fig. 2). These observations are confirmed by radar surveys and by kinematic GPS measurements of tidal motion for the southern flow (Frezzotti and others, 1998a, b). Ice thickness in section CD, close to the grounding line, is 1100–1700 m (Fig. 3c). Radar cross-section CD runs close to the grounding line of the southern flow but, unfortunately, does not cover the entire southern ice flow. Cross-section EF (Fig. 3b) shows the thickness of the northern flow (about 700–900 m) compared to that of the southern flow (1000–1300 m). Radar survey EF runs 10 km downstream of the grounding line of the southern flow and 5 km downstream of the grounding line of the northern flow. The ice velocity close to the grounding line of the southern flow is up to 560 m a^{-1}, whereas the ice velocity of the northern flow is up to 120 m a^{-1} (Fig. 6; Table 1). Ice thickness at the grounding line reaches 1740 m for the southern and 920 m for the northern flow. Ice discharge along transect EF is 5.0 ± 0.2 km^3 a^{-1} for the southern and 0.9 ± 0.1 km^3 a^{-1} for the northern flow. Between radar surveys CD and EF, ice thickness decreases at a rate of 16.4 ± 5.8 m a^{-1} due to basal melting (see next subsection). By summing of basal melting rates, ice-discharge rates were calculated: 6.9 ± 0.6 km^3 a^{-1} for the southern flow (5.0 ± 0.2 km^3 a^{-1} at section EF plus 1.9 ± 0.4 km^3 a^{-1} of basal melting between section EF and the grounding line) and 7.8 ± 0.7 km^3 a^{-1} for both southern and northern flow of David Glacier.

Satellite imagery and radar data show that the grounding line of Mawson Glacier is located at the slope of Mount Murray, about 15 km upstream of the coast. Close to the grounding line, ice thickness (Fig. 5c) reaches 620 m and ice velocity reaches 190 m a^{-1}. Ice discharge is estimated to be 0.52 ± 0.07 km^3 a^{-1} (Fig. 6; Table 1). Frezzotti (1997), based on ice-velocity data derived from satellite tracking and on ice-thickness data reported by Keys and Fowler (1989), calculated an ice discharge of 0.33 ± 0.06 km^3 a^{-1} for Mackay Glacier.

Mass balance

Based on these data, the ice-discharge rate of outlet glaciers is 10.0 ± 1.0 km^3 a^{-1} (Table 1), and, assuming an ice density of 917 kg m^{-3}, we have a value of 9.1 ± 0.9 Gt a^{-1}. Based on ice-discharge rates (9.1 ± 0.9 Gt a^{-1}) for the new catchment area (235 000 km^2) and assuming steady state, a surface-snow accumulation balance of 39 ± 4 kg m^{-2} a^{-1} is estimated. For this area (e-d-d′-D″-E drainage system), Giovinetto and Bentley (1985) and Vaughan and others (1999) reported a net surface accumulation rate on grounded ice of 74 and 97.3 kg m^{-2} a^{-1}, respectively, and a net surface balance of 19.6 and 25.5 Gt a^{-1} using snow-accumulation rates derived from historical snow-pit stratigraphy (Table 2). The ice discharge of outlet glaciers

Table 2. Net surface balance, ice discharge, mean surface accumulation rate and balance snow accumulation of studied area from previous and present analyses

Source	*Grounded drainage area system*	*Mean surface accumulation rate*	*Surface mass balance*
	km^2	kg m^{-2} a^{-1}	Gt a^{-1}
Giovinetto and Bentley (1985)	265 000[(1)]	74	19.6
Vaughan and others (1999)	263 000[(1)]	97.3	25.5
		Balance snow accumulation	*Ice discharge*
		kg m^{-2} a^{-1}	Gt a^{-1}
This study	235 000[(2)]	39 ± 4	9.1 ± 0.9

[(1)] e-d-d′-D″-E drainage system of Giovinetto and Bentley (1985).

[(2)] Priestley, Reeves, David, Mawson, Mackay drainage area.

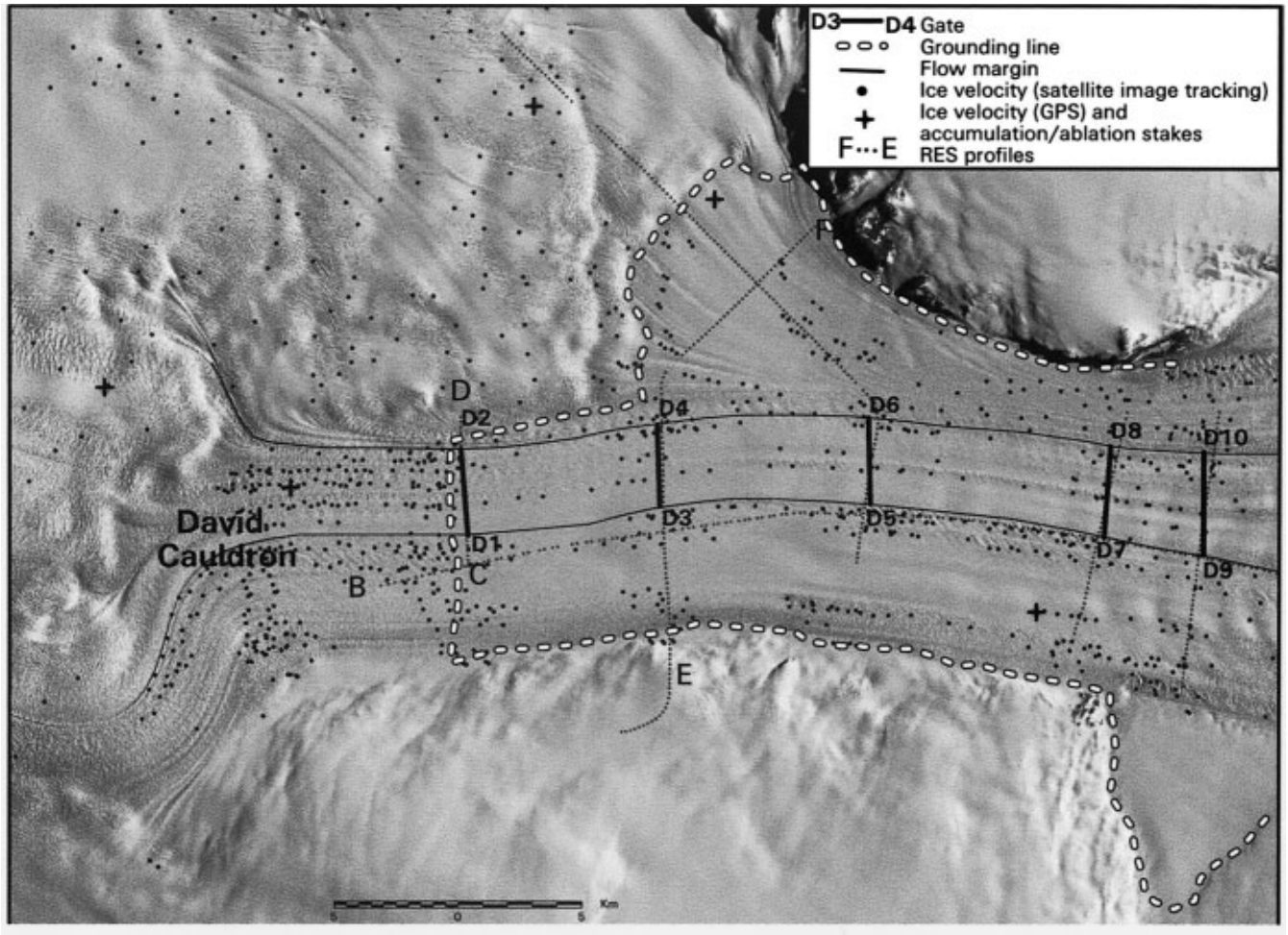

Fig. 7. Landsat TM image of David Glacier with positions and name of RES profiles, velocity data points determined by tracking technique and GPS, location of accumulation/ablation stakes, position and name of gates and flow limits. See Figure 2 for location of this region.

that flow along the Scott Coast is less than half that required for a zero net surface mass balance according to the inputs given by Giovinetto and Bentley (1985) and Vaughan and others (1999). For David Glacier, McIntyre (in Swithinbank, 1988) assessed a balanced discharge of 14 $km^3\ a^{-1}$ for a drainage area of 224 000 km^2. Frezzotti (1997) has estimated iceberg calving ($19.4 \pm 20\%$ Gt a^{-1}) and floating-glacier melting ($20 \pm 50\%$ Gt a^{-1}) for the glaciers that fringe the entire Victoria Land coast. Comparison with Giovinetto and Bentley's (1985) accumulation value ($64.3 \pm 20\%$ Gt a^{-1}) suggests a combined positive mass balance of these glaciers; the imbalance relative to the output flux that Frezzotti (1997) measured represents 37% snow accumulation.

As there is evidence from radar altimetry that the drainage system is not grossly out of steady state (Lingle and Covey, 1998; Rémy and Legrésy, 1998), the explanation for this large apparent imbalance is probably an over estimation of snow accumulation using historical data from snow-pit stratigraphy (1959–60 U.S. Victoria Land Traverse; Stuart and Heine, 1961).

Recent studies of the International Trans-Antarctic Scientific Expedition (ITASE) Italian programme (unpublished information from B. Stenni and others) have revealed an overestimation of snow accumulation in the Talos Dome area. For example, chemical and isotopic analyses of snow–firn cores show accumulation rates up to 50% less than previously reported (Stuart and Heine, 1961); moreover, Cullather and others (1998), using atmospheric moisture budget, have identified low net precipitation along the David, Mackay and Mawson catchment area. The ITASE Italian programme will continue to study the area extending from the coast to Dome C in order to refine the surface mass balance over the entire basin that drains the ice sheet across the Scott Coast.

Floating-glacier discharge flux

Ice-thickness, ice-velocity and accumulation/ablation data from airborne surveys along the floating extensions of the outlet glaciers were collected to study the pattern of basal melting/freezing processes (the glacier is assumed to be in a steady state). The northern flow band of Reeves Glacier within the Nansen Ice Sheet, and the central flow band of David Glacier and Drygalski Ice Tongue were investigated.

The discharge flux of the Reeves flow band was investigated at four gates (Fig. 8) located within 30 km of the grounding line. The flow band is 4.5–6.0 km wide, with average ice thicknesses of 661–271 m and average ice velocities of 113–168 m a^{-1} (Table 3). Blue ice at the surface of the flow band is exposed to katabatic winds. Stake measurements indicate ablation rates ranging from 500 ± 100 kg $m^{-2}\ a^{-1}$ (close to the grounding line) to 400 ± 80 kg $m^{-2}\ a^{-1}$. The rate of change in thickness indicates basal melting values of 0.26 ± 0.92 m a^{-1} from the grounding line (gate R1–R2) to gate R3–R4, 16 km away, and 0.55 ± 0.2 m a^{-1} from gate R3–R4 to gate R5–R6 (Table 3). A basal freezing rate of 0.75 ± 1.83 m a^{-1} was calculated between gate R5–R6 and gate R7–R8. These melting/freezing rates agree with those provided by Frezzotti (1997) for Carnein Glacier (basal melting rate 650–750 kg $m^{-2}\ a^{-1}$) and by Baroni (1990) and Tison and others (1998) for Hells Gate ice shelf (basal freezing rates of 0.10–0.58 m a^{-1}; Figs 2 and 8)

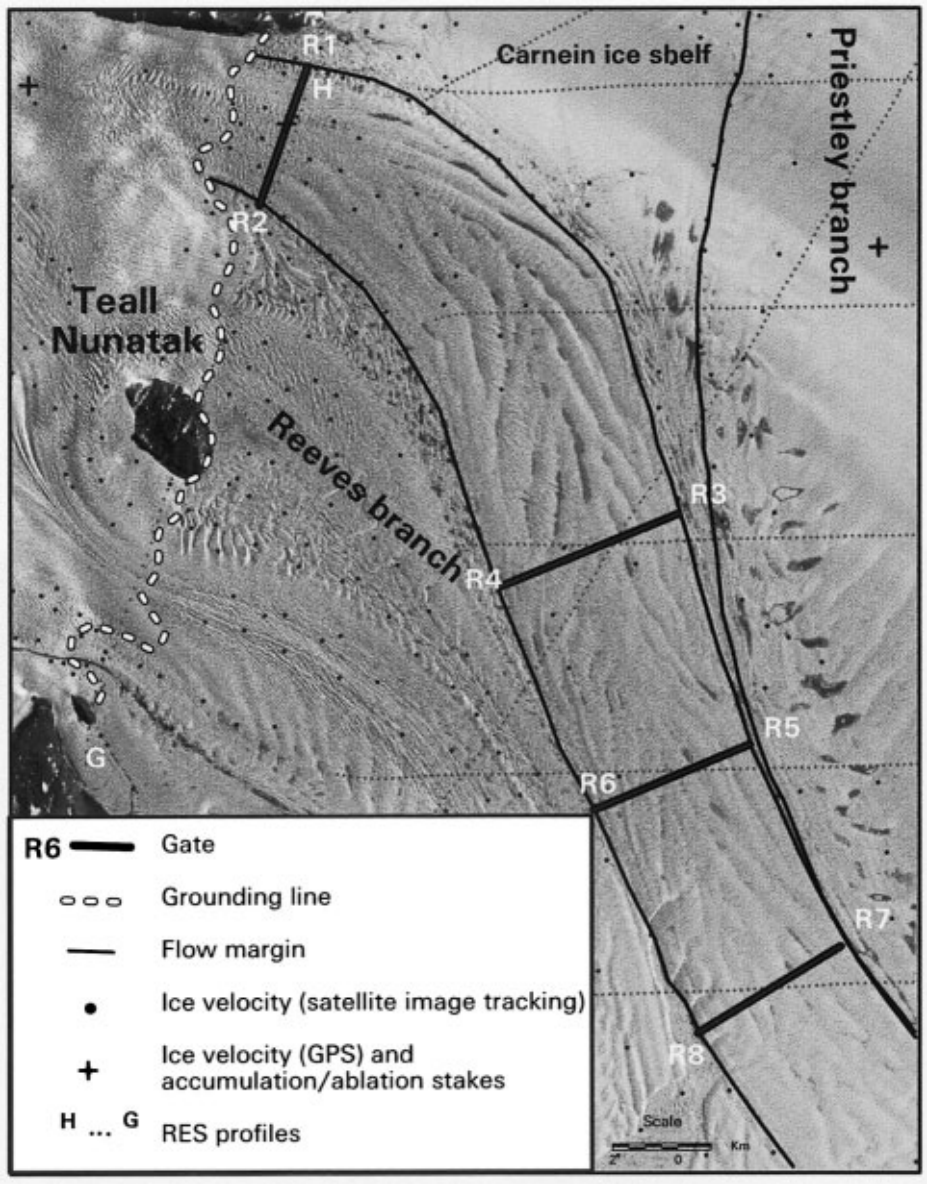

Fig. 8. Landsat TM image of the Nansen Ice Sheet (Reeves branch) with positions and name of RES profiles, velocity data points determined by tracking technique and GPS, location of accumulation/ablation stakes, position and name of gates and flow limits. See Figure 2 for location of this region.

The discharge flux of David–Drygalski Glacier was measured at six gates (Figs 2 and 7) located up to 120 km from the grounding line. The flow band is 3.5–10 km wide, with average ice thicknesses of 1409–197 m and ice velocities of 529–714 m a^{-1} (Table 4). Snow accumulation (measured at stakes) ranges from 50 ± 10 to 185 ± 37 kg m^{-2} a^{-1}. An area with a surface ablation rate of 80 ± 16 kg m^{-2} a^{-1} lies between gates D9–D10 and D11–D12 (Fig. 9). The rate of ice-thickness change ($m - \delta H/\delta t$) ranges from -16.4 ± 5.8 m a^{-1} near the grounding line to $+8.6 \pm 12.0$ m a^{-1} between gates D7–D8 and D9–D10, where the ice tongue leaves the coast (Table 4).

Table 3. Discharge fluxes across flow channels (gates) along the Nansen Ice Sheet and average rate of ice-thickness change as bottom melting–freezing calculated from Equation (2). Data for each gate include width (W), average value of velocity ($\bar{V}_t$), average ice thickness ($\bar{H}$) and ice mass flux computed from Equation (1), surface balance flux (accumulation/ablation) and surface area between gates

Gate	*W*	$\bar{V}_t$	$\bar{H}$	*Flux*	Δ *flux*	*Surface balance rate*	*Surface area*	*Surface flux*	$m - \delta H/\delta t$ *rate of thickness change*
	km	m a^{-1}	m	km^3 a^{-1}	kg m^3 a^{-1}	kg m^{-2} a^{-1}	km^2	km^3 a^{-1}	m a^{-1}
R1–R2	4.5	113	661	0.253 ± 0.037					
					0.23 ± 0.08	-500 ± 100	95	-0.047 ± 0.01	**-0.26 ± 0.9**
R3–R4	6.0	142	304	0.23 ± 0.04					
					0.04 ± 0.07	-400 ± 80	40	-0.016 ± 0.003	**-0.55 ± 0.2**
R5–R6	5.0	155	287	0.192 ± 0.034					
					-0.014 ± 0.07	-400 ± 80	40	-0.016 ± 0.003	**$+0.75 \pm 1.8$**
R7–R8	5.3	168	271	0.206 ± 0.036					

Table 4. Discharge fluxes across flow channels (gates) along David Glacier–Drygalski Ice Tongue and average rate of ice-thickness change as bottom melting–freezing. Data for each gate include width (W), average value of velocity ($\bar{V}_t$), average ice thickness ($\bar{H}$) and ice mass flux computed from Equation (2), surface balance flux (accumulation/ablation) and surface area between gates

Gate	W	$\bar{V}_t$	$\bar{H}$	*Flux*	$\triangle$ *flux*	*Surface balance rate*	*Surface area*	*Surface flux*	$m - \delta H/\delta t$ *rate of thickness change*
	km	m a^{-1}	m	km^3 a^{-1}	kg m^3 a^{-1}	kg m^{-2} a^{-1}	km^2	km^3 a^{-1}	m a^{-1}
D1–D2	3.5	529	1409	2.58 ± 0.086					
					0.457 ± 0.163	50 ± 10	28.0	0.0014 ± 0.0003	**–16.4 ± 5.8**
D3–D4	3.4	520	1163	2.123 ± 0.077					
					0.02 ± 0.156	185 ± 37	28.9	0.0053 ± 0.001	**–0.87 ± 5.4**
D5–D6	3.5	563	1015	2.103 ± 0.079					
					0.306 ± 0.154	185 ± 37	34.1	0.0063 ± 0.0012	**–9.0 ± 4.5**
D7–D8	3.6	594	802	1.797 ± 0.075					
					−0.13 ± 0.185	185 ± 37	15.4	0.0028 ± 0.0006	**+8.6 ± 12.0**
D9–D10	4.1	608	757	1.927 ± 0.11					
						−80 ± 16	209	−0.0167 ± 0.003	
					0.523 ± 0.26				**–1.0 ± 0.5**
						130 ± 26	326	0.042 ± 0.0085	
D11–D12	10.0	714	197	1.404 ± 0.15					

Ice/ocean interaction

Basal melting/freezing processes below floating glaciers of the Terra Nova Bay area have been discussed by various authors (Baroni, 1990; Souchez and others, 1991, 1995; Frezzotti, 1993; Tison and others, 1998). These processes are driven by deep thermohaline circulation triggered by high-salinity shelf water (HSSW) formed as a result of the expulsion of salt during sea-ice formation. Terra Nova polynya is one of the Ross Sea's most important "sea-ice factories", estimated to produce 5–15% of the sea ice generated in the entire Ross Sea shelf (Kurtz and Bromwich, 1985; Frezzotti and Mabin, 1994).

Analyses of thickness variations along the flow bands of David–Drygalski (Fig. 9) and the Nansen Ice Sheet show large uncertainties, but lead to several conclusions about ice/ocean interaction in this region:

(1) David Glacier has a high basal melting rate (16.4 ± 5.8 m a^{-1}) at 1200 m below sea level where ice starts to float, and decreases downstream. The melting rate at the grounding line is higher than previously hypothesized (e.g. Jenkins and Doake, 1991; Jacobs and others, 1992; Frezzotti, 1993) for thermohaline circulation led by HSSW. This high basal melting rate is close to the predicted melting rate for Circumpolar Deep Water intrusion beneath Pine Island Glacier evaluated by Jacobs and others (1996), but far from the basal melting of 50 ± 10 m a^{-1} calculated by Rignot (1998). A high local basal melting rate for David Glacier could be related to over-production of HSSW in the Terra Nova polynya.

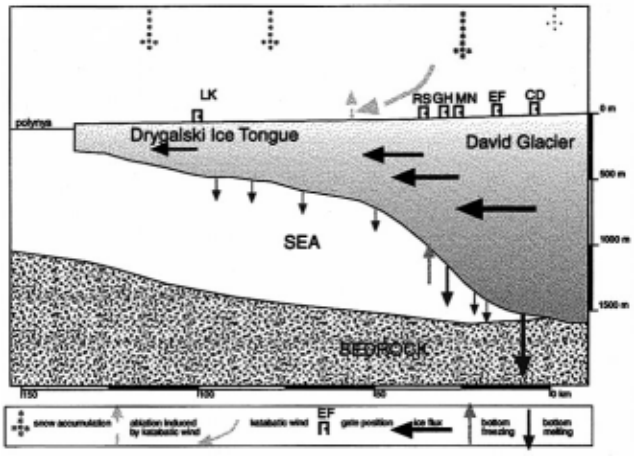

Fig. 9. Schematic sketch of the David Glacier–Drygalski Ice Tongue ice/ocean interaction.

(2) Basal melting at the grounding line of the Reeves flow band is about 10% of that at David Glacier. The grounding line of Reeves Glacier is about 550 m below sea level, much shallower than the deep troughs of David Glacier's southern flow (1200 m below sea level) and Priestley Glacier (about 1000 m below sea level; Fig. 10). The ocean bottom in Terra Nova Bay deepens from the Nansen ice front (700 m below sea level) to the east (about 1000 m below sea level, 5 km from the ice front). The different depths of the grounding lines indicate that David and Priestley Glaciers have deeper sub-ice-shelf cavities which can concentrate HSSW formed in the Terra Nova polynya. This deep-water convection melts large volumes of meteoric ice. The small melting rate at the Reeves grounding line could be linked to intermediate-depth water convection drawn from ice-shelf water (ISW) formed at deeper grounding lines (Priestley and David). The only oceanic profile presently available in Terra Nova Bay (Fabiano and others, 1991) shows ISW from 100 m deep to 600 m above sea floor (700 m deep). This intermediate-depth convection does not melt large volumes of ice (Jacobs and others, 1992).

(3) Basal accretion is present along the David–Drygalski flow band where the bottom ice slope steepens and the floating glacier leaves the valley, in agreement with the previous hypothesis of Frezzotti (1993). Basal accretion is also active along the Reeves Glacier–Nansen Ice Sheet flow band between gates R5–R6 and R7–R8, where the Reeves flow meets the deeper and thicker Priestley flow (600–300 m; Fig. 10). The location of basal freezing agrees with modelling of Deep Thermohaline Convection, which suggests that HSSW evolves into very cold but relatively fresh and light ISW that returns to the ice front. Where the basal slope is steep (where Drygalski Ice Tongue leaves the coast, and the merging area along the Nansen Ice Sheet between the Reeves and Priestley subglacial

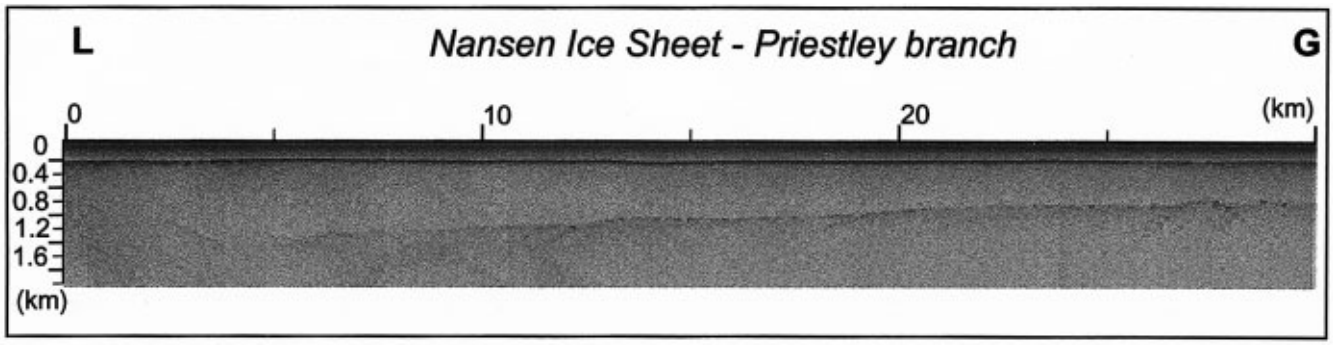

Fig. 10. Radar profiles LG of Nansen Ice Sheet (Priestley branch). Location of profiles in Figure 2.

cave), supercooling of the water mass produces frazil-ice crystals that accrete at the bottom of floating glaciers and slowly consolidate to form marine ice.

The net ablation rates of meteoric ice were estimated from the change in ice thickness along flow channels. About 50% and 25% of the ablation of David and Reeves Glaciers, respectively, is due to basal melting, 50% and 45% to iceberg calving and, for Reeves Glacier, 30% to surface ablation induced by katabatic winds. The 50% melting rate for David Glacier is higher than has been reported by other authors (Jacobs and others, 1992), for whom iceberg calving represents 100–70% of the negative term of the Antarctic mass balance. Estimated mass-loss rates agree with those of Frezzotti (1997), who estimated the iceberg calving flux during the last 50 years for 50 Victoria Land glaciers along 3600 km of coast; he found that mass loss is due to an iceberg calving rate of $19.4 \pm 20\%$ Gt a^{-1} and a floating-glacier melting rate of $20 \pm 50\%$ Gt a^{-1}.

SUMMARY

The combination of satellite-tracking velocity datasets with airborne radar surveys of ice thickness enables calculation of the discharge of Priestley, Reeves, David, Mawson and Mackay outlet glaciers (9.1 ± 0.9 Gt a^{-1}). Using a new DEM constructed by radar altimetry data, the drainage basin of these outlet glaciers is defined and calculated to be 235 000 km^2. The ice discharge of these outlet glaciers is less than half that required for a zero net surface mass balance according to the inputs given by Giovinetto and Bentley (1985) and Vaughan and others (1999). As there is evidence from radar altimetry that the drainage system is not grossly out of steady state, the explanation for this large apparent imbalance is probably an overestimation of snow accumulation using historical data from snow-pit stratigraphy.

The integration of radar and satellite data helped to locate grounding lines; changes in ice fluxes of floating glaciers were used to determine basal melting and freezing rates ranging from -16.4 ± 5.8 to $+8.6 \pm 12.0$ m a^{-1}. The basal melting rates of meteoric ice represent 50% of the net ablation rate for David Glacier. This is higher than the value reported by other authors in Jacobs and others (1992), for whom iceberg calving represents 100–70% of the negative term of the Antarctic mass balance. The high local basal melting rate for David Glacier could be related to over-production of HSSW in the Terra Nova polynya.

ACKNOWLEDGEMENTS

Research was carried out in the framework of a Project on Glaciology and Paleoclimatology of the Programma Nazionale di Ricerche in Antartide, and financially supported by the Ente per le Nuove Tecnologie, l'Energia e l'Ambiente through a cooperation agreement with the Università degli Studi di Milano, and by the European Union under grants ENV4-CT95-0124. Thanks are due to T. Scambos and C. R. Bentley whose comments helped to improve the manuscript.

REFERENCES

Baroni, C. 1990. The Hells Gate and Backstairs Passage ice shelves (Victoria Land, Antarctica). *Mem. Soc. Geol. Ital.*, **43**, 1988, 123–144.

Baroni, C., M. Frezzotti, C. Giraudi and G. Orombelli. 1991. Ice flow and surficial variation inferred from satellite image and aerial photograph analysis of Larsen ice tongue, Hells Gate and Nansen ice shelves (Victoria Land, Antarctica). *Mem. Soc. Geol. Ital.*, **46**, 69–80.

Bentley, C. R. and M. B. Giovinetto. 1991. Mass balance of Antarctica and sea level change. *In* Weller, G., C. L. Wilson and B. A. B. Severin, *eds. International Conference on the Role of the Polar Regions in Global Change: proceedings of a conference held June 11–15, 1990 at the University of Alaska Fairbanks. Vol. II.* Fairbanks, AK, University of Alaska. Geophysical Institute/Center for Global Change and Arctic System Research, 481–488.

Bindschadler, R. A. and T. A. Scambos. 1991. Satellite-image-derived velocity field of an Antarctic ice stream. *Science*, **252**(5003), 242–246.

Bindschadler, R., P. Vornberger, D. Blankenship, T. Scambos and R. Jacobel. 1996. Surface velocity and mass balance of Ice Streams D and E, West Antarctica. *J. Glaciol.*, **42**(142), 461–475.

Cullather, R. I., D. H. Bromwich and M. L. van Woert. 1998. Spatial and temporal variability of Antarctic precipitation from atmospheric methods. *J. Climate*, **11**(3), 334–368.

Drewry, D. J., *ed.* 1983. *Antarctica: glaciological and geophysical folio.* Cambridge, University of Cambridge. Scott Polar Research Institute.

Fabiano, M., P. Povero, G. Catalano and F. Benedetti. 1991. Hydrological data collected during the biological, chemical and geological sampling in Terra Nova Bay. *In Ocean Camp. 1989–90.* Genoa, National Scientific Commission, 35–71.

Frezzotti, M. 1993. Glaciological study in Terra Nova Bay, Antarctica, inferred from remote sensing analysis. *Ann. Glaciol.*, **17**, 63–71.

Frezzotti, M. 1997. Ice front fluctuation, iceberg calving flux and mass balance of Victoria Land glaciers. *Antarct. Sci.*, **9**(1), 61–73.

Frezzotti, M. 1998. Surface wind field of Victoria Land (Antarctica) from surveys of aeolian morphologic features. *Terra Antartica Rep.* 1, 1997, 43–45.

Frezzotti, M. and M. C. G. Mabin. 1994. 20th century behaviour of Drygalski Ice Tongue, Ross Sea, Antarctica. *Ann. Glaciol.*, **20**, 397–400.

Frezzotti, M., C. Baroni and A. Bondesan. 1996. *Glacier and sea-ice features, hydrography.* Siena, Museo Nazionale dell'Antartide. Sezione Scienze della Terra.

Frezzotti, M., A. Capra and L. Vittuari. 1998a. Comparison between glacier ice velocities inferred from GPS and sequential satellite images. *Ann. Glaciol.*, **27**, 54–60.

Frezzotti, M., L. Vittuari and V. Maggi. 1998b. Preliminary GPS measurement of David Glacier and Drygalski ice tongue. *Terra Antartica Rep.* 1, 1997, 13–17.

Giovinetto, M. B. and C. R. Bentley. 1985. Surface balance in ice drainage systems of Antarctica. *Antarct. J. U.S.*, **20**(4), 6–13.

Jacobs, S. S., H. H. Hellmer, C. S. M. Doake, A. Jenkins and R. M. Frolich. 1992. Melting of ice shelves and the mass balance of Antarctica. *J. Glaciol.*, **38**(130), 375–387.

Jacobs, S.S., H. H. Hellmer and A. Jenkins. 1996. Antarctic ice sheet melting in the southeast Pacific. *Geophys. Res. Lett.*, **23**(9), 957–960.

Jenkins, A. and C. S. M. Doake. 1991. Ice–ocean interaction on Ronne Ice Shelf, Antarctica. *J. Geophys. Res.*, **96**(C1), 791–813.

Keys, H. and D. Fowler. 1989. Sources and movement of icebergs in the south-west Ross Sea, Antarctica. *Ann. Glaciol.*, **12**, 85–88.

Kurtz, D. D. and D. H. Bromwich. 1985. A recurring, atmospherically forced polynya in Terra Nova Bay. *In* Jacobs, S. S., *ed. Oceanology of the Antarctic continental shelf*. Washington, DC, American Geophysical Union, 177–201. (Antarctic Research Series 43.)

Lingle, C. S. and D. N. Covey. 1998. Elevation changes on the East Antarctic ice sheet, 1978–93, from satellite radar altimetry: a preliminary assessment. *Ann. Glaciol.*, **27**, 7–18.

Lucchitta, B. K. and H. M. Ferguson. 1986. Antarctica: measuring glacier velocity from satellite images. *Science*, **234**(4780), 1105–1108.

Lucchitta, B. K., K. F. Mullins, A. L. Allison and J. G. Ferrigno. 1993. Antarctic glacier-tongue velocities from Landsat images: first results. *Ann. Glaciol.*, **17**, 356–366.

Lucchitta, B. K., C. E. Rosanova and K. F. Mullins. 1995. Velocities of Pine Island Glacier, West Antarctica, from ERS-1 SAR images. *Ann. Glaciol.*, **21**, 277–283.

McIntyre, N. F. 1985. The dynamics of ice-sheet outlets. *J. Glaciol.*, **31**(108), 99–107.

Morgan, P. J. 1973. A photogrammetric survey of Hoseason Glacier, Kemp Coast, Antarctica. *J. Glaciol.*, **12**(64), 113–120.

Morgan, V. I., T. H. Jacka, G. J. Akerman and A. L. Clarke. 1982. Outlet glacier and mass-budget studies in Enderby, Kemp and Mac. Robertson lands, Antarctica. *Ann. Glaciol.*, **3**, 204–210.

Orombelli, G. 1991. Glaciers and glacial morphology at Terra Nova Bay: an opportunity for significant studies on environmental and climatic global changes. *Mem. Soc. Geol. Ital.*, **46**, 9–16.

Orombelli, G., C. Baroni and G. H. Denton. 1991. Late Cenozoic glacial history of the Terra Nova Bay region, northern Victoria Land, Antarctica. *Geogr. Fis Din. Quat.*, **13**(2), 1990, 139–163.

Rémy, F. and B. Legrésy. 1998. Antarctic non-stationary signals derived from Seasat–ERS-1 altimetry comparison. *Ann. Glaciol.*, **27**, 81–85.

Rémy, F., P. Shaeffer and B. Legrésy. 1999. Ice flow physical processes derived from ERS-1 high-resolution map of Antarctica and Greenland ice sheet. *Geophys. J. Int.*, **139**, 645–656

Rignot, E. J. 1998. Fast recession of a West Antarctic glacier. *Science*, **281**(5376), 549–551.

Souchez, R. *and 7 others*. 1991. Ice composition evidence of marine ice transfer along the bottom of a small Antarctic ice shelf. *Geophys. Res. Lett.*, **18**(5), 849–852.

Souchez, R. *and 6 others*. 1995. Investigating processes of marine ice formation in a floating ice tongue by a high-resolution isotopic study. *J. Geophys. Res.*, **100**(C4), 7019–7025.

Steed, R. H. N. and D. J. Drewry. 1982. Radio-echo sounding investigations of Wilkes Land, Antarctica. *In* Craddock, C., *ed. Antarctic geoscience*. Madison, WI, University of Wisconsin Press, 969–975.

Stuart, A. W. and A. J. Heine. 1961. Glaciological work of the 1959–60 U.S. Victoria Land traverse. *J. Glaciol.*, **3**(30), 997–1002.

Swithinbank, C. 1988. Antarctica. *U.S. Geol. Surv. Prof. Pap.* 1386-B, B1–B138.

Tabacco, I. E., A. Passerini, F. Corbelli and M. Gorman. 1998. Correspondence. Determination of the surface and bed topography at Dome C, East Antarctica. *J. Glaciol.*, **44**(146), 185–191.

Tison, J. -L., R. D. Lorrain, A. Bouzette, M. Dini, A. Bondesan and M. Stiévenard. 1998. Linking landfast sea ice variability to marine ice accretion at Hells Gate Ice Shelf, Ross Sea. *In* Jeffries, M.O., *ed. Antarctic sea ice: physical processes, interactions and variability*. Washington, DC, American Geophysical Union, 375–407. (Antarctic Research Series 74.)

Vaughan, D. G., J. L. Bamber, M. B. Giovinetto, J. Russell and A. P. R. Cooper. 1999. Reassessment of net surface mass balance in Antarctica. *J. Climate*, **12**(4), 933–946.

MS received 14 June 1999 and accepted in revised form 23 November 1999